

October 2021

# Some Thoughts on (the Incompleteness of) the (Double) Differential Event Rates for Elastic WIMP–Nucleus Scattering in (Directional) Direct Dark Matter Detection Physics

CHUNG-LIN SHAN

*Preparatory Office of the Supporting Center for Taiwan Independent Researchers  
P.O.BOX 21 National Yang Ming Chiao Tung University, Hsinchu City 30099, Taiwan, R.O.C.*

*E-mail:* clshan@tir.tw

## Abstract

In this paper, we revisit the expressions for the (double) differential event rates for elastic WIMP–nucleus scattering and discuss some unusual thoughts on (the incompleteness of) the uses of these expressions in (directional) direct Dark Matter detection physics. Several not–frequently mentioned (but important) issues will be argued and demonstrated in detail.

# 1 Introduction

Direct Dark Matter (DM) detection experiments aiming to observe scattering signals of Weakly Interacting Massive Particles (WIMPs) off target nuclei by measuring recoil energies deposited in an underground detector would still be the most reliable experimental strategy for identifying Galactic DM particles and determining their properties [1, 2, 3, 4, 5, 6]. For either providing exclusion limits with null results or reconstructing WIMP properties with positive scattering events, an estimate of the total or the differential event rate for elastic WIMP–nucleus scattering is essential and crucial [1, 3, 4, 6].

During our works on developing the double Monte Carlo scattering–by–scattering simulation procedure of 3-dimensional elastic WIMP–nucleus scattering events [7] as well as studying the 3-D WIMP effective velocity distribution in the Galactic and the Equatorial coordinate systems [8], we revisited the expressions for the (double) differential event rates for elastic WIMP–nucleus scattering used conventionally in (directional) direct DM detection physics. Several incompatibilities between our microscopic and the conventional macroscopic approaches have however been observed.

Hence, in this paper, we would like to discuss these (unusual) thoughts on (the incompleteness of) the expressions for the (double) differential event rates. In Sec. 2, we consider at first the general expression for the differential event rate needed basically in all direct DM detection physics. Then issues of the expression for the double differential event rate used particularly in directional direct detection physics will be argued in Sec. 3. We conclude in Sec. 4.

## 2 Differential event rate

In this section, we discuss at first some possible incompleteness of the differential event rate for elastic WIMP–nucleus scattering.

In literature, the general expression for the differential event rate for elastic WIMP–nucleus scattering used in direct DM detection physics has been given by [1, 3, 4, 6]

$$\frac{dR}{dQ} = \frac{\rho_0}{2m_\chi m_{\text{r,N}}^2} \left[ \sigma_0^{\text{SI}} F_{\text{SI}}^2(Q) + \sigma_0^{\text{SD}} F_{\text{SD}}^2(Q) \right] \int_{v_{\min}(Q)}^{\infty} \left[ \frac{f_1(v_{\chi,\text{Lab}})}{v_{\chi,\text{Lab}}} \right] dv_{\chi,\text{Lab}}. \quad (1)$$

Here  $R$  is the detection event rate,  $Q$  is the nuclear recoil energy deposited in the detector,  $\rho_0$  is the WIMP density near the Earth,  $f_1(v_{\chi,\text{Lab}})$  is the one–dimensional velocity distribution function of the WIMPs *impinging* on the detector,  $v_{\chi,\text{Lab}}$  is the magnitude of the 3-D WIMP incident velocity in the laboratory frame.  $\sigma_0^{(\text{SI},\text{SD})}$  are the spin–independent/dependent (SI/SD) total cross sections ignoring the nuclear form factor suppressions and  $F_{(\text{SI},\text{SD})}(Q)$  indicate the elastic nuclear form factors corresponding to the SI/SD WIMP interactions, respectively.  $m_{\text{r,N}} \equiv m_\chi m_{\text{N}} / (m_\chi + m_{\text{N}})$  is the reduced mass of the WIMP mass  $m_\chi$  and that of the target nucleus  $m_{\text{N}}$ . Finally,  $v_{\min}(Q)$  is the minimal–required incoming velocity of incident WIMPs that can deposit the energy  $Q$  in the detector:

$$v_{\min}(Q) = \sqrt{\frac{m_{\text{N}}}{2m_{\text{r,N}}^2}} \sqrt{Q}. \quad (2)$$

### 2.1 Recoil–angle dependence of the recoil energy

In Fig. 1 we sketch a WIMP–nucleus ( $\chi$ –N) scattering event with a WIMP incident velocity of  $v_{\chi,\text{Lab}}$ .  $\zeta$  is the scattering angle of the outgoing WIMP,  $\eta$  is the recoil angle of the scattered target

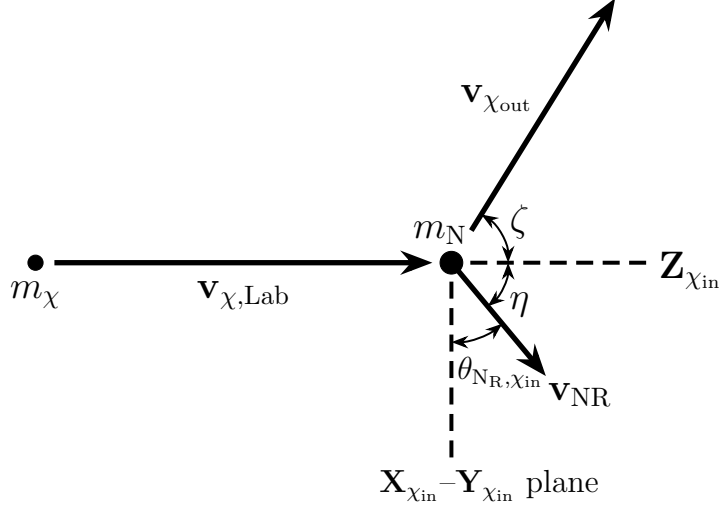


Figure 1: The sketch of a WIMP–nucleus ( $\chi$ –N) scattering event with a WIMP incident velocity of  $v_{\chi, \text{Lab}}$ .  $\zeta$  is the scattering angle of the outgoing WIMP,  $\eta$  is the recoil angle of the scattered target nucleus, and  $\theta_{\text{NR}, \chi_{\text{in}}} = \pi/2 - \eta$  is the elevation of the recoil direction of the scattered nucleus (the equivalent recoil angle) in the incoming–WIMP ( $\chi_{\text{in}}$ ) coordinate system [7]. The  $\mathbf{Z}_{\chi_{\text{in}}}$ –axis is defined as the direction of the incoming velocity of the incident WIMP  $\mathbf{v}_{\chi, \text{Lab}}$ .

nucleus, and  $\theta_{\text{NR}, \chi_{\text{in}}} = \pi/2 - \eta$  is the elevation of the recoil direction of the scattered nucleus (the “equivalent” recoil angle) in the incoming–WIMP ( $\chi_{\text{in}}$ ) coordinate system [7]. While  $m_{\chi}$  indicates (the mass of) the incident WIMP,  $m_{\text{N}}$  is (the mass of) the scattered target nucleus in our detector.

The kinetic energy of the incident WIMP with the incoming velocity of  $\mathbf{v}_{\chi, \text{Lab}}$  in the laboratory (detector rest) coordinate system can be given by

$$E_{\chi} = \frac{1}{2} m_{\chi} |\mathbf{v}_{\chi, \text{Lab}}|^2 = \frac{1}{2} m_{\chi} v_{\chi, \text{Lab}}^2. \quad (3)$$

Then the recoil energy of the scattered target nucleus can be expressed as a function of the recoil angle  $\eta$  as [9, 10, 2]

$$Q(v_{\chi, \text{Lab}}, \eta) = \left[ \frac{4m_{\chi}m_{\text{N}}}{(m_{\chi} + m_{\text{N}})^2} \cos^2(\eta) \right] E_{\chi} = \left( \frac{2m_{\text{r}, \text{N}}^2}{m_{\text{N}}} \right) v_{\chi, \text{Lab}}^2 \cos^2(\eta), \quad (4)$$

where  $m_{\text{r}, \text{N}}$  is the reduced mass given above.

Conventionally, for a given recoil energy  $Q_{\text{h}}$  (see Fig. 2(b)), people use Eq. (4) with the minimal recoil angle of  $\eta = 0$  (namely, Eq. (2)) to define the minimal–required incoming velocity  $v_{\text{min}, \text{h}} \equiv v_{\text{min}}(Q_{\text{h}})$  appearing as the lower bound of the integral in Eq. (1). Then, for estimating the differential event rate  $(dR/dQ)_{Q=Q_{\text{h}}}$ , we integral over the 1-D velocity distribution function  $f_1(v_{\chi, \text{Lab}})$  (divided by  $v_{\chi, \text{Lab}}$ ) from  $v_{\text{min}, \text{h}}$  to a maximal cut–off velocity of incident WIMPs in the Equatorial/laboratory coordinate systems ( $v_{\chi, \text{cutoff}} \simeq 800$  km/s) by assuming implicitly that *the velocity distribution of the “scattering” WIMPs (moving with velocities larger than  $v_{\text{min}, \text{h}}$ ) is exactly identical to the 1-D velocity distribution of “incident” halo WIMPs,  $f_1(v_{\chi, \text{Lab}})$ ,*<sup>1</sup> and ignoring the dependence of the recoil energy on the recoil angle  $\eta$  through Eq. (4), as along the upper solid (blue) line shown in Fig. 2(b). This implies in practice that, for another recoil energy  $Q_1 < Q_{\text{h}}$  with the corresponding minimal WIMP–incoming velocity  $v_{\text{min}, \text{l}} \equiv v_{\text{min}}(Q_1)$ , the

<sup>1</sup>See Refs. [8, 11] for detailed discussions and demonstrations against this assumption.

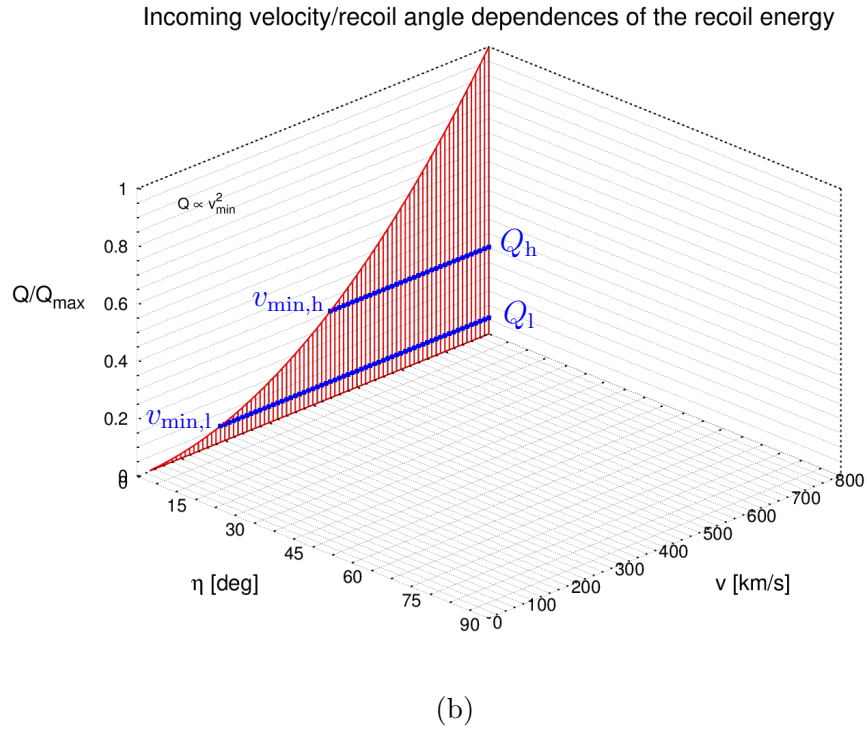
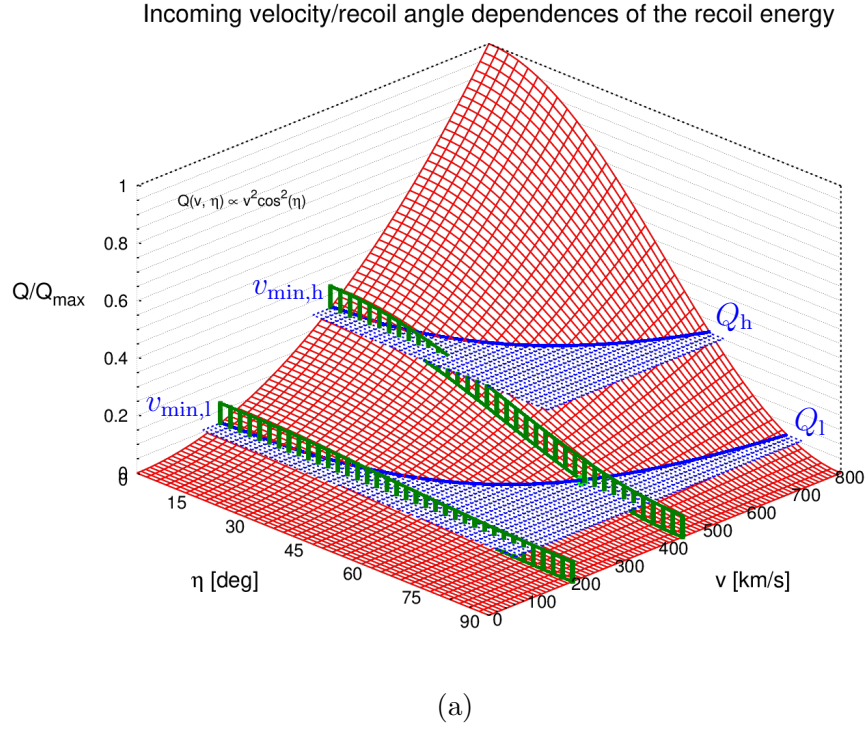


Figure 2: (a) The 2-D dependence of the recoil energy on the WIMP incident velocity  $v_{\chi, \text{Lab}}$  and the recoil angle  $\eta$  given in Eq. (4). (b) The projection of the recoil-energy surface on the  $\eta = 0$  plane. See the text for detailed descriptions and discussions.

predicted contribution of incident WIMPs moving with velocities  $v_{\chi,\text{Lab}} \geq v_{\min,h}$  to the differential event rate  $(dR/dQ)_{Q=Q_1}$  would exactly be equal to that to  $(dR/dQ)_{Q=Q_h}$ . Additionally, for different target nuclei, as long as the lower bounds of the integral are equal (to e.g.  $v_{\min,h}$  or  $v_{\min,l}$ ), the predicted contributions of the integral to the differential event rates (around different recoil energies!) would also be equal.

However, since the recoil energy depends on not only the WIMP incident velocity  $v_{\chi,\text{Lab}}$  but also the nuclear recoil angle  $\eta$ , we would need to consider a 2-D surface as shown in Fig. 2(a). For the given recoil energy  $Q_h$ , the integral in the differential event rate  $(dR/dQ)_{Q=Q_h}$  should go along the upper (dark-blue) intersection path of the (red)  $Q(v_{\chi,\text{Lab}}, \eta)$  surface and the (blue) “equal-recoil-energy- $Q_h$ ” plane. This means that the contribution of the integral in the range of  $v_{\chi,\text{Lab}} \geq v_{\min,h}$  to  $(dR/dQ)_{Q=Q_h}$  would be totally different from the contribution of the integral to  $(dR/dQ)_{Q=Q_1}$  (the lower (dark-blue) intersection path). This would then make (the expression for) the estimate of the differential event rate (much) more complicated. Below, in the rest part of this section, we provide from the theoretical point of view the most important (but may not be usually considered) arguments for it<sup>2</sup>.

First of all, as shown in Fig. 2(a), for the given WIMP incident velocity  $v_{\min,h}$  (the upper (dark-green) vertical fence), one could consider reversely the corresponding recoil energy  $Q_h$  as the “maximal transferable” recoil energy to the scattered target nucleus:

$$Q_{\max}(v_{\min,h}) \equiv \left( \frac{2m_{\text{r},\text{N}}^2}{m_{\text{N}}} \right) v_{\min,h}^2 = Q_h. \quad (5)$$

Then, for any recoil angle  $\eta > 0$ , the larger the recoil angle  $\eta$  (along downwards the upper (dark-green) vertical fence), the smaller the corresponding recoil energy  $Q(v_{\chi,\text{Lab}} = v_{\min,h}, \eta > 0)$ . As will be discussed in detail in Sec. 2.2, this implies a *weaker* cross section (nuclear form factor) suppression and thus possibly a *larger* scattering probability. Hence, incident WIMPs moving with  $v_{\chi,\text{Lab}} = v_{\min,h}$  would (much) more likely scatter off a target nucleus with a larger recoil angle  $\eta^* = \cos^{-1} \left( \sqrt{Q_1/Q_h} \right)$  (the green point) and thus transfer the given recoil energy  $Q_1$ . This indicates from so far only the nuclear-form-factor point of view clearly that head-on scattering events should be (much) rarer than people thought before.

In fact, for all  $v_{\chi,\text{Lab}} \geq v_{\min,h}$ , it would always be more possible to observe scattering events with lower recoil energy  $Q_1$  and larger recoil angles than those with higher energy  $Q_h$  and smaller recoil angles. Hence, it would be pretty hard to believe that the contributions of the integrals along two intersection paths of the equal-recoil-energy- $Q_h/Q_1$  planes from  $v_{\chi,\text{Lab}} = v_{\min,h}$  to the cut-off WIMP incident velocity  $v_{\chi,\text{cutoff}}$  to the differential event rates  $(dR/dQ)_{Q=Q_h}$  and  $(dR/dQ)_{Q=Q_1}$  would be identical<sup>3</sup>.

Moreover, as will be argued in more details in Sec. 2.3, the scattering probability at different incident velocity-recoil angle  $(v_{\chi,\text{Lab}}-\eta)$  combinations depends partially on the nuclear form factor, which depends on detector materials and the WIMP mass. Thus, for estimating the differential event rate  $dR/dQ$ , the form factors  $F_{(\text{SI},\text{SD})}(Q)$  would need to be *included inside* the integral and handled as functions of the incident velocity  $v_{\chi,\text{Lab}}$  and the recoil angle  $\eta$  through Eq. (4).

---

<sup>2</sup>A detailed investigation on the (target and WIMP-mass dependent) incident velocity-recoil angle distribution for elastic WIMP-nucleus scattering in different (small) energy windows will be announced later [11].

<sup>3</sup>In Ref. [11], we will demonstrate that the “effective” velocity distributions of scattering WIMPs inducing recoil energies in different (small) energy windows would be clearly different and (much) more complicated than target and WIMP-mass dependent.

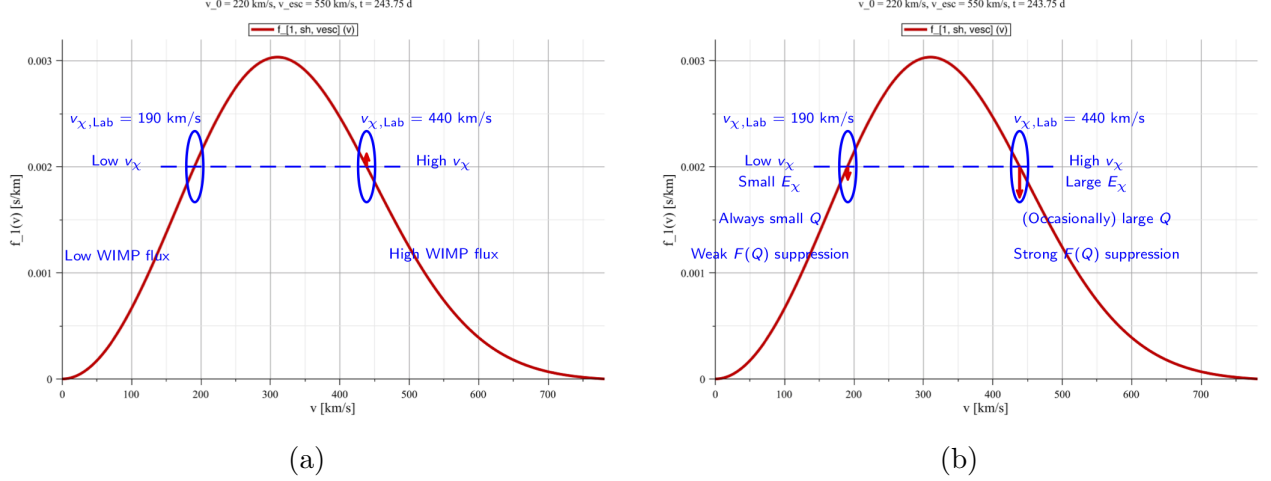


Figure 3: Two factors which affect the dependence of the WIMP–nucleus scattering probability on the WIMP incident velocity: (a) the proportionality of the WIMP flux to the incident velocity, (b) the nuclear form factor suppression depending on the induced recoil energy, which is proportional to the kinetic energy of the scattering WIMP. The solid red curves are the shifted Maxwellian velocity distribution given in Eq. (7) of Ref. [8]. See the text for detailed arguments. (Figures from Ref. [8]).

## 2.2 Cross section (nuclear form factor) suppression

In the previous Sec. 2.1, we have mentioned the dependence of the WIMP scattering probability on the cross section (nuclear form factor). In this subsection, we discuss the effects of the nuclear form factor suppression on the scattering probability in more details.

Given the mass of incident WIMPs and the detector target nucleus, as sketched in Figs. 3, the scattering probability of incident halo WIMPs moving with different incoming velocities depends on two factors: (a) the WIMP flux is proportional to the incident velocity  $v_{\chi,\text{Lab}}$ , and (b) the recoil angle and thus the recoil energy is constrained by the nuclear form factor suppression.

The first factor of the flux proportionality to the WIMP incident velocity (sketched in Fig. 3(a)) is easy to understand (and was already considered in the differential event rate (1)): the higher (lower) the incoming velocity of incident WIMPs, the more (fewer) the target nuclei passed by an incident WIMP (in a unit time) and thus the larger (smaller) the scattering opportunity.

On the other hand, as sketched on the left-hand side of Fig. 3(b), for WIMPs moving with low incident velocities and thus only carrying small kinetic energies, the maximal transferable recoil energies to target nuclei are small and the nuclear form factor suppression as well as the reduction of the scattering probability are weak or even negligible, especially when light nuclei are used as detector materials *or* the WIMP mass is light (see also Figs. 4). In contrast, for WIMPs moving with high incident velocities and thus carrying large kinetic energies (the right-hand side of Fig. 3(b)), the transferable recoil energies to target nuclei are also large and the nuclear form factor suppression as well as the reduction of the scattering probability become (pretty) strong, especially when heavy nuclei are used *and* the WIMP mass is heavy.

As readers' reference, in Fig. 4(a), we provide the recoil-energy dependence of the nuclear form factors corresponding to the SI (solid) and the SD (dash-dotted) cross sections adopted in our simulation package [7]. Five frequently used target nuclei have been considered:  $^{19}\text{F}$  (blue),  $^{40}\text{Ar}$  (green),  $^{73}\text{Ge}$  (red),  $^{129}\text{Xe}$  (black), and  $^{183}\text{W}$  (magenta). The sharply enlarged form factor

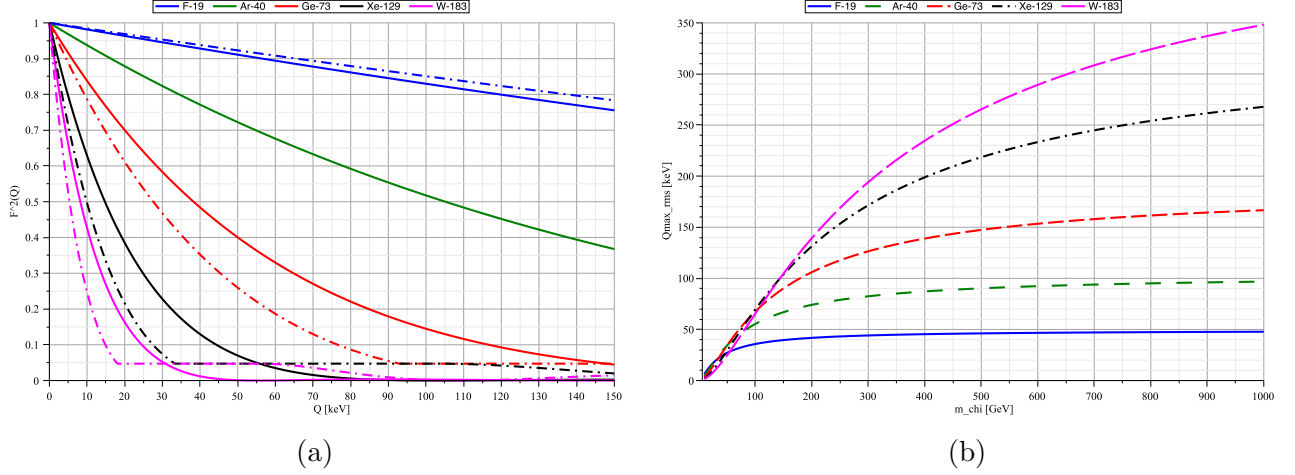


Figure 4: (a) Nuclear form factors of the  $^{19}\text{F}$  (blue), the  $^{40}\text{Ar}$  (green), the  $^{73}\text{Ge}$  (red), the  $^{129}\text{Xe}$  (black), and the  $^{183}\text{W}$  (magenta) nuclei (adopted in our simulation package [7]) as functions of the recoil energy. The solid and the dash-dotted curves indicate the form factors corresponding to the SI and the SD cross sections, respectively. (b) The WIMP-mass dependence of the maximal recoil energy  $Q_{\text{max,rms}}$  given by Eq. (6). Five frequently used target nuclei:  $^{19}\text{F}$  (solid blue),  $^{40}\text{Ar}$  (rare-dashed green),  $^{73}\text{Ge}$  (dashed red),  $^{129}\text{Xe}$  (dash-dotted black), and  $^{183}\text{W}$  (long-dashed magenta) have been considered. (Figures from Ref. [7]).

suppressions with the increased mass of the target nucleus can be seen clearly. Moreover, as auxiliary material, Fig. 4(b) shows the WIMP-mass dependence of the maximal transferable recoil energy with the root-mean-square velocity of incident halo WIMPs estimated by Eq. (40) of Ref. [7]:

$$Q_{\text{max,rms}} = \left( \frac{2m_{\text{r,N}}^2}{m_{\text{N}}} \right) v_{\text{rms,Lab}}^2, \quad (6)$$

for five frequently used target nuclei:  $^{19}\text{F}$  (solid blue),  $^{40}\text{Ar}$  (rare-dashed green),  $^{73}\text{Ge}$  (dashed red),  $^{129}\text{Xe}$  (dash-dotted black), and  $^{183}\text{W}$  (long-dashed magenta). This indicates clearly that, due to the nuclear form factor suppression, especially for heavy target nuclei like  $^{129}\text{Xe}$  and  $^{183}\text{W}$ , even though the WIMPs are not very heavy and the incoming velocities are not very high, the transferable recoil energy would be pretty large and thus the scattering probability should be pretty strongly reduced.

As will be discussed in detail in Sec. 2.3 (and Ref. [11]), this implies further that the deviation of the most frequent recoil angle from the zero recoil angle (head-on scattering) could be pretty large, especially when the target nuclei *and* incident WIMPs are heavy [11].

### 2.3 Recoil-angle dependence of the differential scattering cross section

In literature, given a WIMP incident velocity  $v_{\chi,\text{Lab}}$ , the differential scattering cross section  $d\sigma$  is given by the absolute value of the momentum transfer from the incident WIMP to the scattered nucleus as [1, 3, 4, 6]

$$d\sigma = \frac{1}{v_{\chi,\text{Lab}}^2} \left( \frac{1}{4m_{\text{r,N}}^2} \right) \left[ \sigma_0^{\text{SI}} F_{\text{SI}}^2(q) + \sigma_0^{\text{SD}} F_{\text{SD}}^2(q) \right] dq^2$$

$$= \frac{1}{v_{\chi,\text{Lab}}^2} \left( \frac{m_N}{2m_{\text{r},N}^2} \right) \left[ \sigma_0^{\text{SI}} F_{\text{SI}}^2(Q) + \sigma_0^{\text{SD}} F_{\text{SD}}^2(Q) \right] dQ, \quad (7)$$

where we have

$$q = \sqrt{2m_N Q}. \quad (8)$$

Since, as shown in Eq. (4), the recoil energy  $Q$  is a “one-to-one” function of the recoil angle  $\eta$  (given the WIMP incident velocity  $v_{\chi,\text{Lab}}$ ), the differential cross section  $d\sigma$  of incident halo WIMPs with an incoming velocity  $v_{\chi,\text{Lab}}$  off target nuclei going into a recoil angle of  $\eta \pm d\eta/2$  with a recoil energy of  $Q \pm dQ/2$  can further be expressed as [7]

$$d\sigma = - \left[ \sigma_0^{\text{SI}} F_{\text{SI}}^2(Q) + \sigma_0^{\text{SD}} F_{\text{SD}}^2(Q) \right] \sin(2\eta) d\eta. \quad (9)$$

Here the “minus (−)” sign indicates that the recoil energy  $Q$  decreases while the recoil angle  $\eta$  increases. Note that, although, with the zero recoil angle  $\eta = 0$ , the corresponding recoil energy  $Q(v_{\chi,\text{Lab}}, \eta = 0) \propto v_{\chi,\text{Lab}}^2$  is maximal, the differential recoil energy  $dQ \propto \sin(2\eta) = 0$  as well as the differential cross section  $d\sigma = 0$ . This indicates that an “exact head-on” elastic WIMP–nucleus scattering event is actually *impossible*!

Moreover, by combining Eqs. (9) and (4), one can have that

$$\left| \frac{d\sigma}{d\eta} \right| = \left[ \sigma_0^{\text{SI}} F_{\text{SI}}^2(Q) + \sigma_0^{\text{SD}} F_{\text{SD}}^2(Q) \right] \sin(2\eta), \quad (10)$$

and

$$Q(v_{\chi,\text{Lab}}, \eta) \left| \frac{d\sigma}{d\eta} \right| = 2 \left[ \left( \frac{2m_{\text{r},N}^2}{m_N} \right) v_{\chi,\text{Lab}}^2 \right] \left[ \sigma_0^{\text{SI}} F_{\text{SI}}^2(Q) + \sigma_0^{\text{SD}} F_{\text{SD}}^2(Q) \right] \cos^3(\eta) \sin(\eta). \quad (11)$$

Hence, ignoring the nuclear form factor suppression, one can obtain the lower bounds of the most frequent and the most energetic recoil angles of  $\eta_{\text{bound}} = 45^\circ$  and  $\eta_{Q,\text{bound}} = 30^\circ$ , respectively, at which  $|d\sigma/d\eta|$  and  $Q(\eta)|d\sigma/d\eta|$  are maximal [12].

In Figs. 5 and 6, we show the normalized recoil-angle dependence of  $|d\sigma/d\eta|$  and the corresponding recoil-angle dependence of  $Q(\eta)|d\sigma/d\eta|$  given in Eqs. (10) and (11), respectively. Five frequently used target nuclei:  $^{19}\text{F}$  (solid blue),  $^{40}\text{Ar}$  (rare-dashed green),  $^{73}\text{Ge}$  (dashed red),  $^{129}\text{Xe}$  (dash-dotted black), and  $^{183}\text{W}$  (long-dashed magenta) and three different WIMP masses:  $m_\chi = 20, 100$ , and  $500$  GeV have been considered<sup>4</sup>. The form factors corresponding to the SI and the SD cross sections adopted in our simulation package have been used [7]. Note that these curves are WIMP-velocity dependent and the root-mean-square velocity of halo WIMPs estimated by Eq. (40) of Ref. [7] has been considered again here.

In these plots, the target and WIMP-mass dependent shifts of the most frequent and the most energetic recoil angles towards larger  $\eta$ ’s caused by the nuclear form factor suppression can be seen obviously. This implies that, for different target nuclei, even with the same WIMP incident velocity, the scattering probability at each incident velocity–recoil angle ( $v_{\chi,\text{Lab}}-\eta$ ) combination along the intersection paths of the equal-recoil-energy planes shown in Fig. 2(a) and thus the contributions to the differential event rate  $dR/dQ$  would be different [11].

<sup>4</sup>Interested readers can click each plot in Figs. 5 and 6 to open the corresponding webpage of the animated demonstration of detailed Monte Carlo simulation results with varying target nuclei (for more considered WIMP masses) (see Ref. [12] for detailed discussions). Note however that all recoil-angle-dependence plots shown in our demonstration webpage [13] are given as functions of the equivalent recoil angle  $\theta_{\text{NR},\chi_{\text{in}}} = \pi/2 - \eta$ .

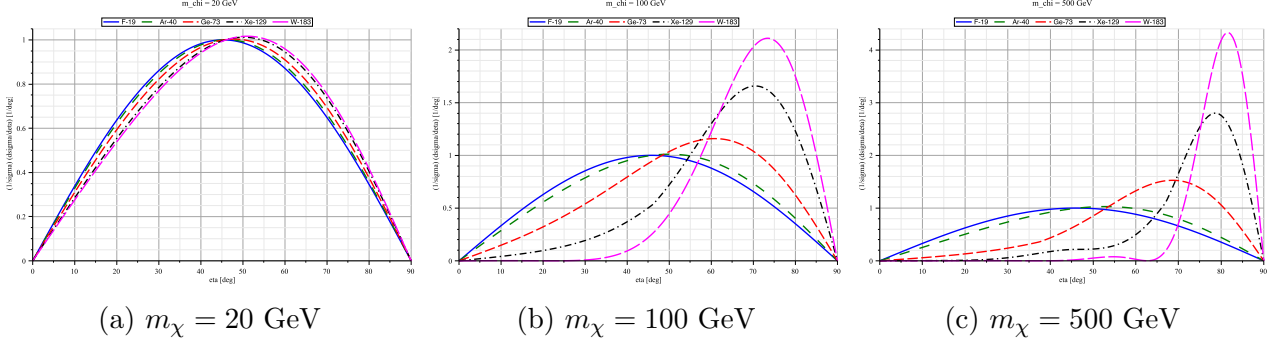


Figure 5: The normalized recoil-angle dependence of  $|d\sigma/d\eta|$  given in Eq. (10) for five frequently used target nuclei:  $^{19}\text{F}$  (solid blue),  $^{40}\text{Ar}$  (rare-dashed green),  $^{73}\text{Ge}$  (dashed red),  $^{129}\text{Xe}$  (dash-dotted black), and  $^{183}\text{W}$  (long-dashed magenta). Three different WIMP masses have been considered. The form factors corresponding to the SI and the SD cross sections adopted in our simulation package have been used [7]. The WIMP incident velocity here has been assumed (monotonically) as the root-mean-square velocity of halo WIMPs estimated by Eq. (40) of Ref. [7].

Finally, it would be important to argue that, from Eq. (10), one can also find that

$$\left| \frac{d\sigma}{d\Omega} \right| = \frac{d\eta}{d\Omega} \left| \frac{d\sigma}{d\eta} \right| = \frac{1}{2\pi \sin(\eta)} \left| \frac{d\sigma}{d\eta} \right| = \frac{1}{\pi} \left[ \sigma_0^{\text{SI}} F_{\text{SI}}^2(Q) + \sigma_0^{\text{SD}} F_{\text{SD}}^2(Q) \right] \cos(\eta). \quad (12)$$

It seems thus to imply that the WIMP-induced nuclear recoil flux has a maximum at the zero-recoil-angle direction. However, it is actually just because that  $d\Omega = 2\pi \sin(\eta)d\eta$  is infinitesimal at  $\eta = 0$ .

It would also be worth to remind here that what we have discussed in this subsection indicates the importance of the form of the interaction(s) between incident WIMPs (Dark Matter particles) and the target nuclei (scattered ordinary particles) in the estimate of the scattering event rate (and, consequently, the determination of the exclusion limit or WIMP/DM properties), in particular, the relation between the recoil energy and the recoil angle (i.e., the kinematics of WIMP/DM scattering). Hence, in other DM-interaction scenarios (e.g. DM-electron scattering, cosmic-ray boosted DM, etc.), similar expressions for estimating the scattering event rates would also need to be revisited.

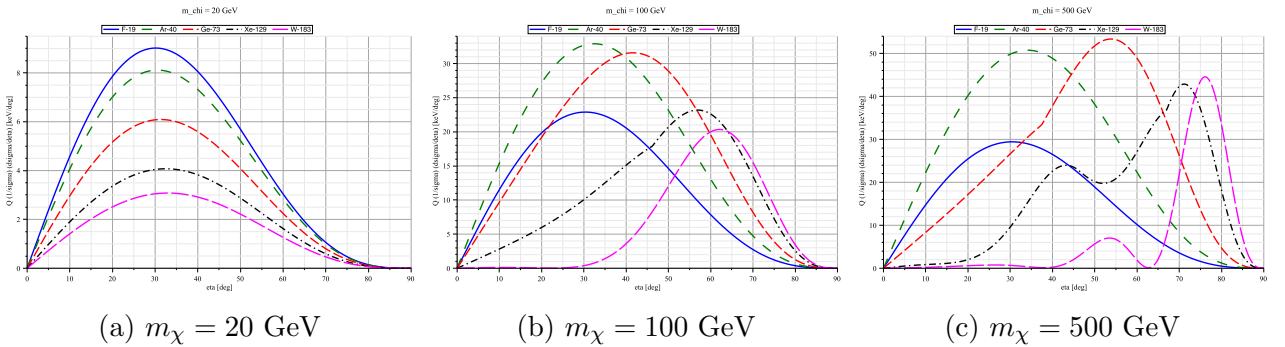


Figure 6: Corresponding to Figs. 5: the recoil-angle dependence of  $Q(\eta)|d\sigma/d\eta|$  given in Eq. (11) for five frequently used target nuclei with three different WIMP masses. Notations as in Figs. 5.

## 2.4 1-D WIMP effective velocity distribution

By taking into account the flux proportionality to the WIMP incident velocity, the scattering probability distribution of incident halo WIMPs *with a given incoming velocity*  $v_{\chi,\text{Lab}}$  off target nuclei going into a recoil angle of  $\eta \pm d\eta/2$  in a recoil energy window of  $Q \pm dQ/2$  can generally be expressed by [7]

$$f_{\text{NR},\chi\text{in}}(v_{\chi,\text{Lab}}, \eta) = \frac{v_{\chi,\text{Lab}}}{v_{\chi,\text{cutoff}}} \left| \frac{d\sigma}{d\eta} \right| = \frac{v_{\chi,\text{Lab}}}{v_{\chi,\text{cutoff}}} \left[ \sigma_0^{\text{SI}} F_{\text{SI}}^2(Q) + \sigma_0^{\text{SD}} F_{\text{SD}}^2(Q) \right] \sin(2\eta). \quad (13)$$

Then, as argued in Sec. 2.2 and demonstrated in Ref. [8], due to the nuclear form factor suppression appearing as the second (bracket) factor in Eq. (13), the actual “effective” velocity distribution of incident halo WIMPs *scattering off* target nuclei should be (much) more strongly reduced from the theoretical prediction in the high velocity range than in the low velocity range, once the target nuclei and incident WIMPs are heavy. This reduction could however be balanced by the (first) factor of the flux proportionality to the WIMP incident velocity in Eq. (13). Consequently, the “effective” average and root-mean-square velocities of light (heavy) WIMPs (impinging on and) scattering off light (heavy) target nuclei should be larger (smaller) than those of the entire Galactic halo WIMPs [8].

However, in a standard derivation of the differential event rate (1) given in, e.g. Ref. [1], the average velocity of incident halo WIMPs:

$$\langle v \rangle = \int_0^\infty v f_1(v) dv, \quad (14)$$

has been adopted directly for estimating the flux of the incident and also the “scattering” WIMPs needed in  $dR/dQ$ . As argued above, for a given WIMP incident velocity but different recoil energies (on different equal-recoil-energy planes in Fig. 2(a)), the scattering probability of different corresponding recoil angles and the contribution to the differential event rate should be different. This indicates that, even if one consider to use an average velocity as a macroscopical description/approximation for incident velocities of the “scattering” WIMPs, a modified effective velocity distribution depending on the considered recoil energy (as well as on the target nucleus and the WIMP mass) would be needed (see Ref. [11] for detailed numerical simulation results).

Finally, it would be worth to note that the scattering probability given in Eq. (13) (including the nuclear form factor in the bracket and the recoil angle term of  $\sin(2\eta)$ ) would need to be included inside the integral over the velocity distribution function in Eq. (1) and the integral would need to cover all possible incident velocity–recoil angle combination.

## 3 Double differential event rate

In this section, we discuss then the double differential event rate used in directional direct DM detection physics.

In literature, the expression for the double differential event rate for elastic WIMP–nucleus scattering has been given by [14, 15, 10, 2, 16, 17]

$$\begin{aligned} \frac{d^2 R}{dQ d\Omega_{\hat{\mathbf{q}}}} &= \frac{\rho_0}{4\pi m_\chi m_{\text{r,N}}^2} \left[ \sigma_0^{\text{SI}} F_{\text{SI}}^2(Q) + \sigma_0^{\text{SD}} F_{\text{SD}}^2(Q) \right] \\ &\times \int_{v_{\min}(Q)}^\infty \delta \left( \mathbf{v}_{\chi,\text{Lab}} \cdot \hat{\mathbf{q}} - \frac{q}{2m_{\text{r,N}}} \right) f(\mathbf{v}_{\chi,\text{Lab}}) d^3 \mathbf{v}_{\chi,\text{Lab}}. \end{aligned} \quad (15)$$

Here  $\Omega_{\hat{\mathbf{q}}}$  is the solid angle around the recoil direction  $\hat{\mathbf{q}}$  with the recoil angle  $\eta$  and the  $\delta$ -function ensures that, for an incident WIMP moving with a given velocity  $v_{\chi,\text{Lab}} \geq v_{\min}(Q)$  and transferring energy  $Q$  to a nucleus in our detector, the recoil angle of the scattered target nucleus  $\eta$  satisfies that

$$\mathbf{v}_{\chi,\text{Lab}} \cdot \hat{\mathbf{q}} = v_{\chi,\text{Lab}} \cos \eta = \frac{q}{2m_{\text{r},\text{N}}} = \sqrt{\frac{m_{\text{N}}}{2m_{\text{r},\text{N}}^2}} \sqrt{Q}. \quad (16)$$

For the use of the double differential event rate given in Eq. (15), it seems that one not only assumes implicitly *again* that the velocity distribution of the “scattering” WIMPs (moving with velocities larger than  $v_{\min}(Q)$ ) obeys exactly the 1-D velocity distribution of “incident” halo WIMPs in the Equatorial/laboratory frames, but also *ignores the recoil-angle dependence of the differential scattering cross section* given in Eq. (9). Then, for the considered recoil energy  $Q \pm dQ/2$ , the angular distribution of the recoil flux is determined by Eq. (16) with incident velocities constrained by the WIMP velocity distribution.

However, ...

### 3.1 (Only) the relation between the WIMP incident and the nuclear recoil directions

The double differential event rate (15) seems to describe only the relation between the WIMP incident and the nuclear recoil directions. Namely, considering at first the case that all incident WIMPs move (almost) identically in one common direction, only the recoil angles of the scattering events matter and the angular distribution of the recoil flux would be displayed with the azimuthal symmetry around this common direction.

However, once we consider two bunches of WIMPs moving in two different common directions, the situation seems to become unsolvable. Giving an energy window of  $Q \pm dQ/2$ , according to Eq. (15), the first bunch of WIMPs moving with different velocities would induce nuclear recoils in different rings centered at the first common direction of the incident velocities; so the second bunch of WIMPs and the induced nuclear recoils. The question now is: how could we combine these two recoil distribution patterns? And, with the third, the forth recoil distribution patterns?

Unfortunately, ...

### 3.2 WIMP incident directions would not be (highly) concentrated

In literature, (for practical uses of the double differential event rate (15),) it is often to consider the opposite direction of the movement of the Solar system in our Galaxy, namely, the direction from the Cygnus constellation to the Solar center, as a reference direction and assume that the incident velocities of halo WIMPs highly concentrate around this direction of the so-called “WIMP wind” [15, 2, 17, 5].

However, the real situation should more likely be that described by R. J. Creswick *et al.* [18]:

*“Several effects mitigate against a strong correlation between the distribution of recoils and the direction of the WIMP wind. First, the velocity  $\mathbf{v}$  of the WIMP is the vector sum of the fixed wind  $\mathbf{w}$  and a random virial velocity,  $\mathbf{u}$ , of roughly equal magnitude. Hence at any given time the direction of the WIMP impinging upon the crystal has a broad distribution that is only peaked around  $\mathbf{w}$ . The directionality effect is further diluted by the recoil of the elastically scattered nucleus, which we assume is isotropic in the CM frame<sup>5</sup>. Finally, the directionality effect is further reduced by the nuclear form factor, relevant for heavier nuclei, which suppresses scattering a high momentum transfer.”*

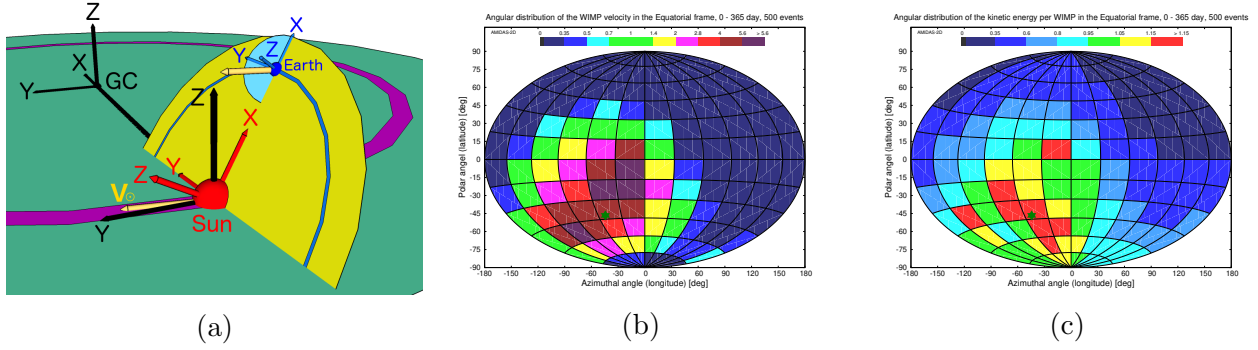


Figure 7: (a) The movement of the Solar system around the Galactic center (GC) (along the magenta circular path), which points currently towards the Cygnus constellation (indicated by the golden arrows). The relative orientations between the black Galactic, the red Ecliptic, and the blue Equatorial coordinate systems (on the date of the vernal equinox) have also been sketched, whereas the blue circular band (on the yellow Ecliptic plane) indicates the Earth’s orbit around the Sun. (Figure from Ref. [19]). (b)(c) The simulated angular distributions of the WIMP incident flux and the “average WIMP kinetic energy” (in unit of the all-sky average values) in the Equatorial coordinate system, respectively. 500 simulated WIMP velocities on average (Poisson distributed) in one entire year have been recorded and binned into  $12 \times 12$  bins for the azimuthal angle and the elevation, respectively. The dark-green stars indicate the opposite direction of the Solar Galactic movement [20]:  $42.00^\circ\text{S}$ ,  $50.70^\circ\text{W}$ . Note that the scales of the color bars are different. (Figures from Refs. [19] and [21], respectively).

In the Galactic point of view, the moving directions of incident WIMPs should be random and (approximately) isotropic, then (vector) added by the movement of the Solar system (or, more precisely, that of the Earth or even the laboratory) to return the incoming directions in the laboratory frame. Hence, the WIMP incident flux should indeed center at (very closely to) the direction from the Cygnus constellation to the Solar center. However, its decreasing distribution would not be ring-like around the center but rather distorted.

In Fig. 7(a), the golden arrows indicate the movement of the Solar system around the Galactic center (along the magenta circular path), which points currently towards the Cygnus constellation. We show also the relative orientations between the (black) Galactic, the (red) Ecliptic, and the (blue) Equatorial coordinate systems (on the date of the vernal equinox) [19]. Then we simulated 500 *isotropic* WIMP velocities on average (Poisson distributed) in the Galactic coordinate system in one entire year and transformed them to the Equatorial coordinate system [19, 7]. Their angular distribution is shown in Fig. 7(b) (in unit of the all-sky average value). The dark-green star indicates the opposite direction of the Solar Galactic movement in the Equatorial coordinate system [20]:  $42.00^\circ\text{S}$ ,  $50.70^\circ\text{W}$ . It can be found interestingly that, while the intense area (directions) of the WIMP incident flux covers indeed the opposite direction of the Solar Galactic movement, it distributes rather *obliquely* from the center towards the southwest corner of the sky [19].

On the other hand, the simulated angular distribution of the “average kinetic energy” of incident WIMPs (in unit of the all-sky average value) in the Equatorial coordinate system in Fig. 7(c) shows that, firstly, in contrast to the obliquely-distributed intense area of the WIMP incident flux, the main hot spot of the average WIMP kinetic energy spreads longitudinally

<sup>5</sup>From this isotropy of the recoil angle in the “center-of-mass” frame [6], one can derive directly the recoil-angle dependence (9) of the differential cross section to the differential recoil angle in the “laboratory” frame.

through the opposite direction of the Solar Galactic movement [21]. Secondly and surprisingly, two extra peaks appear near the center and the southwest corner of the sky [21].

These simulation results demonstrate clearly that, even though the WIMP Galactic velocity distribution has been here most simply assumed as isotropic, the angular distribution of the 3-D velocity of WIMPs impinging on our detectors would already be more complicated than a highly concentrated WIMP wind<sup>6</sup>.

Furthermore, ...

### 3.3 WIMP-induced nuclear recoils could be strongly deflected from the WIMP-wind direction

Probably because that, with a given recoil energy  $Q$ , for calculating the minimal-required incoming velocity of incident WIMPs,  $v_{\min}(Q)$ , by Eq. (4), the zero-recoil-angle ( $\eta = 0$ ) condition has been used, or because that  $d\sigma/d\Omega$  given in Eq. (12) indicates that the differential WIMP-nucleus scattering cross section per unit solid angle has a maximum when  $\eta = 0$ , in literature, e.g. Refs. [9, 22, 10, 23, 24, 2, 16, 25, 17, 5], it has very frequently been asserted that the most possible WIMP-induced events would be “head-on” scattering and thus the angular distribution of the recoil flux of the scattered target nuclei would peak opposite to the direction of the movement of the Solar system/Earth. Additionally, in e.g. Refs. [9, 10, 2, 17], the authors have even presented ring-like-decreased recoil-flux distributions centered at the direction of the Cygnus constellation/WIMP wind (estimated probably by using the double differential event rate (15)).

However, as argued and demonstrated in several different ways in Sec. 2, firstly, due to the *zero* differential cross section at zero recoil angle, the recoil direction of the scattered target nucleus will definitely not along the incident direction of the scattering WIMP. Instead, due to the lower bound and the increase of the most frequent recoil angle (with the increasing target and/or WIMP mass), the deviation of the nuclear recoil direction from that of the incident scattering WIMP could be pretty large. For heavy target nuclei like  $^{129}\text{Xe}$  and  $^{183}\text{W}$  (as well as  $^{127}\text{I}$  and  $^{133}\text{Cs}$ ), a large number of recoil events could even be deflected almost perpendicularly (see Figs. 5(b) and (c)).

Moreover, as demonstrated in Sec. 3.2, the angular distribution of the WIMP incident flux in the Equatorial coordinate system should be more complicated than that of a highly concentrated WIMP-wind. This makes the “superposition” of the nuclear recoil fluxes induced by WIMPs coming (anisotropically) from all directions much more complicated than a simple ring-like-decreased distribution centered around the theoretical WIMP-wind direction.

In Figs. 8 and 9, we show the angular distributions of the WIMP-induced nuclear recoil flux and the corresponding average recoil energy (per event) observed in the Equatorial coordinate system (in unit of the all-sky average values), respectively. WIMPs of three different masses scatter off three different target nuclei have been presented: (a) 20-GeV WIMPs off  $^{19}\text{F}$ , (b) 100-GeV WIMPs off  $^{73}\text{Ge}$ , (c) 500-GeV WIMPs off  $^{129}\text{Xe}$ . 500 accepted scattering events on average (Poisson distributed) in one entire year have been recorded<sup>7</sup>.

It can be seen clearly that the angular recoil-flux distributions of all three considered WIMP mass-target nucleus combinations would not (exactly) center at the theoretical direction of the WIMP wind (the dark-green star). The heavier the incident WIMPs and/or the target nucleus,

<sup>6</sup>As demonstrated in Ref. [8], the 3-D (radial and angular) distribution of the “effective” velocity distribution of WIMPs *scattering off* target nuclei in both of the Galactic and the Equatorial coordinate systems would be much more complicated and depend on target material and the WIMP mass.

<sup>7</sup>Interested readers can click each plot in Figs. 8 and 9 to open the corresponding webpage of the animated demonstration with varying WIMP masses (for more considered target nuclei).

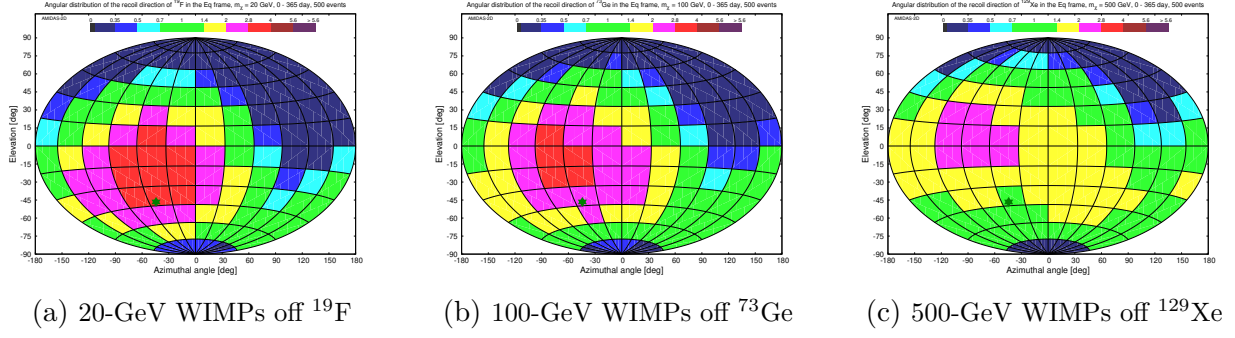


Figure 8: The angular distributions of the WIMP-induced nuclear recoil flux observed in the Equatorial coordinate system (in unit of the all-sky average value). WIMPs of three different masses scatter off three different target nuclei have been presented. 500 accepted scattering events on average (Poisson distributed) in one entire year have been recorded. (Figures from Refs. [12, 13]).

the larger the northern deviation of the peak of the nuclear recoil flux. In contrast, the angular distributions of the average recoil energy of all three considered WIMP mass-target nucleus combinations seem to peak approximately around the theoretical WIMP-wind direction, with nevertheless some small (but observable) WIMP-mass and target dependent pattern differences.

More detailed discussions about the angular distributions of the recoil flux and the (average) recoil energy of the WIMP-scattered target nuclei in different celestial coordinate systems can be found in Refs. [12, 26]. And in Ref. [11], we will present the angular recoil-flux distributions with different WIMP mass-target nucleus combinations in different small (a few keV) recoil energy windows.

### 3.4 3-D WIMP (effective) velocity distributions

At the end of this section, we would like to mention that a technical difficulty in using the double differential event rate (15) would be about an analytic functional form of the 3-D WIMP velocity distribution in more realistic (and thus complicated) models of the Dark Matter halo,

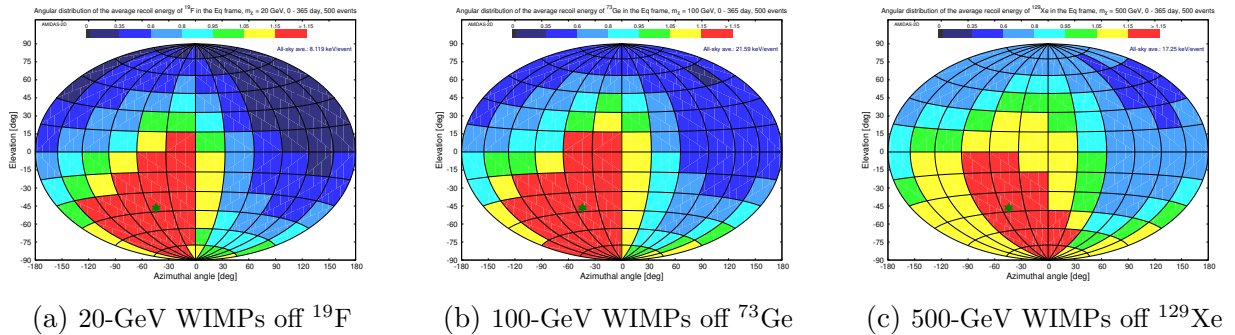


Figure 9: Corresponding to Figs. 8: the angular distributions of the average recoil energy (per event) observed in the Equatorial coordinate system (in unit of the all-sky average values). Note that the all-sky average values depend on the WIMP mass and the target nucleus and thus are different in three plots. (Figures from Refs. [12, 13]).

in particular, when one wants to include Dark Matter stream(s) [10].

Moreover, as demonstrated in Ref. [8] and mentioned in Sec. 2.4, due to the combination of the flux proportionality to the WIMP incident velocity and the (target and WIMP-mass dependent) nuclear form factor suppression, one needs to consider the 3-D “effective” velocity distribution of halo WIMPs scattering off target nuclei, even when the simplest isotropic (Maxwellian) velocity distribution in the Galactic coordinate system is adopted. This makes the situation much more complicated.

## 4 Summary

In this paper, we discussed some unusual thoughts on (the incompleteness of) the expressions for the (double) differential event rates for elastic WIMP-nucleus scattering used in (directional) direct Dark Matter detection physics by comparing the commonly used expressions with those used in our double Monte Carlo scattering-by-scattering simulation procedure.

Considering an incident WIMP moving with a given incident velocity and scattering off a target nucleus, one can find that the smaller the recoil angle, since the larger the corresponding recoil energy and thus the stronger the nuclear form factor suppression, the smaller the scattering probability could be. More precisely, the recoil-angle dependence of the differential scattering cross section with respect to the differential recoil angle indicates that head-on (zero-recoil-angle) WIMP-nucleus scattering should be impossible. Instead, WIMP signals with large recoil angles should be observed more frequently than we thought earlier and, caused by the nuclear form factor suppression, the ratio of large-recoil-angle events should increase with the increasing target and/or WIMP mass.

On the other hand, regarding the use of the double differential event rate in directional detection physics, we argued and demonstrated at first that, although the incident WIMP flux centers approximately at the opposite direction of the Solar Galactic movement, its decreasing distribution would not be ring-like around the center but rather distorted. Moreover, combined with the large-angle deflection of the WIMP-induced nuclear recoils, our numerical simulations show clearly that the angular distribution of the recoil flux of the WIMP-scattered target nuclei should be more complicated than the conventionally-believed ring-like-decreased distribution centered around the direction of the theoretically predicted WIMP wind. Once our target nuclei and the mass of incident WIMPs are pretty heavy, the angular recoil-flux distribution could be flattened (pretty) widely and the maximum could shift away (largely) from the WIMP-wind direction. Detailed investigations on the (target and WIMP-mass dependent) incident velocity-recoil angle distribution for elastic WIMP-nucleus scattering as well as the corresponding angular recoil-flux distributions will be announced soon.

In summary, several not-frequently mentioned (but important) issues in (directional) direct DM detection physics have been argued and demonstrated in this work in detail. Unfortunately, we have so far no concrete suggestions for their alterations. We hope nevertheless that this work could initiate our colleagues to reconsider our theories/assumptions as well as earlier works in this field and eventually find out suitable improvements.

## Acknowledgments

The author would like to thank the pleasant atmosphere of the Cancer Center of the Kaohsiung Veterans General Hospital, where part of this work was completed. This work was strongly encouraged by the “*Researchers working on e.g. exploring the Universe or landing on the Moon should not stay here but go abroad.*” speech.

## References

- [1] G. Jungman, M. Kamionkowski and K. Griest, “*Supersymmetric Dark Matter*”, *Phys. Rept.* **267**, 195–373 (1996), [arXiv:hep-ph/9506380](#).
- [2] F. Mayet *et al.*, “*A Review of the Discovery Reach of Directional Dark Matter Detection*”, *Phys. Rept.* **627**, 1–49 (2016), [arXiv:1602.03781 \[astro-ph.CO\]](#).
- [3] M. Schumann, “*Direct Detection of WIMP Dark Matter: Concepts and Status*”, *J. Phys.* **G46**, 103003 (2019), [arXiv:1903.03026 \[astro-ph.CO\]](#).
- [4] L. Baudis and S. Profumo, contribution to “*The Review of Particle Physics 2020*”, *Prog. Theor. Exp. Phys.* **2020**, 083C01 (2020), 27. Dark Matter.
- [5] S. E. Vahsen, C. A. J. O’Hare and D. Loomba, “*Directional Recoil Detection*”, *Ann. Rev. Nucl. Part. Sci.* **71**, 189–224 (2021), [arXiv:2102.04596 \[physics.ins-det\]](#).
- [6] J. Cooley, “*Dark Matter Direct Detection of Classical WIMPs*”, [arXiv:2110.02359 \[hep-ph\]](#) (2021).
- [7] C.-L. Shan, “*Monte Carlo Scattering-by-Scattering Simulation of 3-Dimensional Elastic WIMP–Nucleus Scattering Events*”, [arXiv:2103.06485 \[hep-ph\]](#) (2021), in publication.
- [8] C.-L. Shan, “*3-Dimensional Effective Velocity Distribution of Halo Weakly Interacting Massive Particles Scattering off Nuclei in Direct Dark Matter Detectors*”, [arXiv:2103.06883 \[astro-ph.HE\]](#) (2021), in publication.
- [9] J. Billard, F. Mayet, J. F. Macias–Perez and D. Santos, “*Directional Detection as a Strategy to Discover Galactic Dark Matter*”, *Phys. Lett.* **B691**, 156–162 (2010), [arXiv:0911.4086 \[astro-ph.CO\]](#).
- [10] C. A. J. O’Hare and A. M. Green, “*Directional Detection of Dark Matter Streams*”, *Phys. Rev.* **D90**, 123511 (2014), [arXiv:1410.2749 \[astro-ph.CO\]](#).
- [11] C.-L. Shan, “*Incident Velocity–Recoil Angle Distribution and Angular Recoil Energy Spectrum of 3-Dimensional WIMP–Nucleus Scattering Events*” (temporary), [arXiv:2203.0nnnn \[hep-ph\]](#) (2022), in finalization.
- [12] C.-L. Shan, “*Simulations of the Angular Recoil–Energy Distribution of WIMP–Scattered Target Nuclei for Directional Dark Matter Detection Experiments*”, [arXiv:2103.06486 \[hep-ph\]](#) (2021), in publication.
- [13] C.-L. Shan, online interactive demonstrations of 3-dimensional elastic WIMP–nucleus scattering for (directional) direct Dark Matter detection experiments and phenomenology, <http://www.tir.tw/phys/hep/dm/amidas-2d/> (2021).
- [14] P. Gondolo, “*Recoil Momentum Spectrum in Directional Dark Matter Detectors*”, *Phys. Rev.* **D66**, 103513 (2002), [arXiv:hep-ph/0209110](#).
- [15] J. Billard, F. Mayet and D. Santos, “*A Markov Chain Monte Carlo Analysis to Constrain Dark Matter Properties with Directional Detection*”, *Phys. Rev.* **D83**, 075002 (2011), [arXiv:1012.3960 \[astro-ph.CO\]](#).

- [16] C. A. J. O’Hare, B. J. Kavanagh and A. M. Green, “*Time–Integrated Directional Detection of Dark Matter*”, *Phys. Rev.* **D96**, 083011 (2017), [arXiv:1708.02959](#) [[astro-ph.CO](#)].
- [17] CYGNUS Collab., S. E. Vahsen *et al.*, “*CYGNUS: Feasibility of a Nuclear Recoil Observatory with Directional Sensitivity to Dark Matter and Neutrinos*”, [arXiv:2008.12587](#) [[physics.ins-det](#)] (2020).
- [18] R. J. Creswick, S. Nussinov and F. T. Avignone, “*Direction Dependence and Diurnal Modulation in Dark Matter Detectors*”, *Astropart. Phys.* **35**, 62–66 (2011), [arXiv:1007.0214](#) [[astro-ph.IM](#)].
- [19] C.-L. Shan, “*Simulations of the 3-Dimensional Velocity Distribution of Halo Weakly Interacting Massive Particles for Directional Dark Matter Detection Experiments*”, [arXiv:1905.11279](#) [[astro-ph.HE](#)] (2019), in publication.
- [20] A. Bandyopadhyay and D. Majumdar, “*On Diurnal and Annual Variations of Directional Detection Rates of Dark Matter*”, *Astrophys. J.* **746**, 107 (2012), [arXiv:1006.3231](#) [[hep-ph](#)].
- [21] C.-L. Shan, “*Simulations of the Angular Kinetic–Energy Distribution of Halo Weakly Interacting Massive Particles for Directional Dark Matter Detection Experiments*”, in publication.
- [22] A. M. Green and B. Morgan, “*The Median Recoil Direction as a WIMP Directional Detection Signal*”, *Phys. Rev.* **D81**, 061301 (2010), [arXiv:1002.2717](#) [[astro-ph.CO](#)].
- [23] C. A. J. O’Hare, A. M. Green, J. Billard, E. Figueroa–Feliciano and L. E. Strigari, “*Read-out Strategies for Directional Dark Matter Detection beyond the Neutrino Background*”, *Phys. Rev.* **D92**, 063518 (2015), [arXiv:1505.08061](#) [[astro-ph.CO](#)].
- [24] Q. Riffard *et al.*, “*MIMAC Low Energy Electron–Recoil Discrimination Measured with Fast Neutrons*”, *J. Inst.* **11**, P08011 (2016), [arXiv:1602.01738](#) [[astro-ph.IM](#)].
- [25] CYGNO Collab., E. Baracchini *et al.*, “*A 1 m<sup>3</sup> Gas Time Projection Chamber with Optical Readout for Directional Dark Matter Searches: the CYGNO Experiment*”, [arXiv:2001.02453](#) [[physics.ins-det](#)] (2020).
- [26] C.-L. Shan, “*Annual Modulations of the Angular Recoil–Flux/Energy Distributions of WIMP–Scattered Target Nuclei Observed at an Underground Laboratory*”, *proceedings of the 17th International Conference on Topics in Astroparticle and Underground Physics (TAUP 2021)*, [arXiv:2110.05027](#) [[hep-ph](#)] (2021).